Hyperbranched epoxy and carbon dot nanohybrid based nanocomposites

Highlight

This chapter deals with fabrication, characterization and property evaluation of thermosetting nanocomposites of hyperbranched epoxy with carbon dot based nanohybrid. It contains two sub-chapters, where in the first sub-chapter a highly tough thermostable hyperbranched epoxy nanocomposite was fabricated by the incorporation of carbon dot reduced Cu_2O nanohybrid, which exhibited efficient reusable photocatalytic activity towards the degradation of pesticide under solar light. This high performance nanocomposite with photocatalytic attribute has strong potential to be used as a functional thin film material, as well as thermostable reusable photocatalyst. The second sub-chapter deals with mechanical, thermal, antimicrobial and optical property evaluation of a biocide immobilized OMMT-carbon dot reduced Cu_2O nanohybrid/hyperbranched epoxy nanocomposite. The nanocomposite exhibited high transparency, excellent performance with interesting antimicrobial and photoluminescence attributes. Thus, the work contributes a light in the field of advanced antimicrobial functional thermosetting material.

Parts of this chapter are published in

1. B. De, B. Voit and N. Karak, *RSC Adv*. **4**, 58453-58459, 2014.
2. B. De, K. Gupta, M. Mandal and N. Karak, *Mater. Sci. Eng. C* **56**, 74-83, 2015.

5A. Hyperbranched epoxy/carbon dot reduced Cu_2O nanocomposites

5A.1. Introduction

Different zero dimentional metal and metal oxide nanoparticles like copper, copper oxides, silver, gold, titanium oxide, zinc oxide, etc. are widely used in polymer nanocomposites to achieve various interesting properties like optical, electrical, antimicrobial, catalysis and so on, as mentioned in the first chapter.[1-8] Metal oxide nanoparticles like TiO_2, ZnO, Cu_2O, etc. are extensively used as photocalysts for degradation of organic pollutants.[5-8] Photocatalysis is one of the greenest approaches for the destruction of different hazardous anthropogenic organic contaminants.[4,7-9] This is because of the fact that the photodegradation of the contaminants is economically favorable and the process is fast even at their very low concentration under ambient conditions. However, in most of the cases used catalysts, semiconductor quantum dots and metal oxide nanoparticles are toxic in nature and catalytic efficiency at visible light are also very low.[6,10-12] Further, among the different hazardous anthropogenic organic chemicals, pesticides are the most common non-degradable anthropogenic chemical contaminants both in water and soil.[10,13] They are extensively used in industry as well as in agriculture. Organophosphates like paraoxon are mainly used as nerve agents, chemical warfare agents as well as pesticides and insecticides in agriculture.[14,15] They enter into the water and cause convulsions and respiratory paralysis by prolongation of cholinergic effects to the living system.[14] However, degradation of pesticide by nanophotocatalyst is limited and the efficiency of such reported catalysts is very poor even under UV irradiation.[14] In this respect, attributes like low-toxicity, easy availability, low cost, p-type semiconductor with a direct band gap of 2.2 eV, photocatalytic activity under visible light and others endow Cu_2O nanoparticles a unique position in the domain of metal oxide based photocatalyst.[7,8,16] But, preparation and stabilization of Cu_2O nanoparticles are the major issues as in maximum cases Cu_2O nanoparticles are formed with mixture of Cu and CuO nanoparticles.[17,18] Therefore, a control reduction of Cu^{2+} or oxidation of Cu^0 to Cu_2O nanoparticles is necessary and the process is critical. In this vein, carbon dot may reduce metal salts in a controlled manner and one pot such reduction are gaining importance in recent times.[19] Recently, it is also intensively used as a photocatalyst because of its tunable emissions from near-infrared to blue wavelength.[20] Again, researchers designed carbon dot with other metal or metal oxide nanoparticles for enhancing catalytic efficiency by exploiting the up-conversion luminescence properties of it.[8,20,21] Furthermore, control reduction of Cu^{2+}

and stabilization of Cu_2O can be performed in presence of suitable stabilizing agents. In this context, polymer supported heterogeneous catalyst (polymer nanocomposite) is an attractive option. Polymer matrix not only acts as a stabilizer of the catalyst, it also offers reusability and easy handling of the catalyst.[3,5] High thermostability, high mechanical strength, excellent chemical resistance as well as infusible and insoluble nature of the epoxy thermoset offer it as one of the best matrices for this purpose.

Therefore, in the present sub-chapter, a carbon dot reduced Cu_2O nanohybrid/hyperbranched epoxy nanocomposite was used as a tough and thermostable reusable photo-catalyst for the degradation of pesticide under solar light. Carbon dot offers simultaneous improvement in strength, toughness and thermal stability of the thermoset after formation of nanocomposites as observed in Chapter 4.

5A.2. Experimental

5A.2.1. Materials

In this sub-chapter same hyperbranched epoxy (TAHE20) was used like previous chapters. Here used carbon dot was also prepared from banana juice as described in sub-chapter 4A. Cupric acetate [$Cu(OAc)_2$] monohydrate was used for the preparation of Cu_2O nanoparticles by reduction with carbon dot. It was purchased from Rankem, India. Ethyl paraoxon pesticide was used in photocatalytic reaction as it is one of the most common non-degradable anthropogenic chemical contaminants both in water and soil, and largely used in industry as well as in agriculture. It was obtained from Sigma Aldrich, Germany. All other chemicals like solvents, PAA hardener, etc. were used in this sub-chapter were same as described in the previous chapters.

5A.2.2. Characterization

The instrumentation and characterization techniques for spectroscopic, microscopic, XRD, mechanical and thermal testing were same as reported previous chapters. Here only the intensity of the solar light was measured by using a lux meter (LX-101, Lutron, Taiwan).

5A.2.3. Methods

5A.2.3.1. Preparation of carbon dot reduced Cu_2O nanohybrid

Carbon dot reduced Cu_2O nanohybrid was prepared by reduction of cupric acetate solution in ethanol by carbon dot. In a typical process, 0.5 g of $Cu(OAc)_2$ was dissolved in 25 mL of EtOH by stirring 15 min in a two necked round bottom flask. A 20 mL aqueous solution of

NH_3 (30%) was added to the above solution and stirred another 15 min at room temperature to form copper ammonium complex. Then a water-condenser was equipped with round bottom flask and temperature was raised to 70 °C. At this temperature, a 25 mL ethanolic solution of carbon dot (0.5 g) was added drop wise to the mixture. The mixture was continuously stirred for 6 h at the same temperature. After completion of the reaction, the solution was allowed to cool down naturally and separation of the nanohybrid particles was done by ultracentrifugation at 5000 rpm for 10 min. The particles were washed with EtOH for 2-3 times and then dispersed in 20 mL EtOH by ultrasonication for 5 min.

5A.2.3.2. Preparation of nanocomposites with hyperbranched epoxy

Carbon dot reduced Cu_2O nanohybrid/hyperbranched epoxy nanocomposites were prepared by solution technique as described in the sub-chapter 4B, section 4B.2.3. Briefly, the desired amount (0.5, 1.0 and 1.5 wt% compared to hyperbranched epoxy) of EtOH dispersed carbon dot reduced Cu_2O nanohybrid was added into hyperbranched epoxy resin and stirred magnetically for 2 h at room temperature followed by ultrasonication for 10 min under similar conditions as described in sub-chapter 4B. A 50 wt% of poly(amido-amine) (PAA) was mixed homogeneously with the above mixture and coated on glass plates. Before curing the plates were kept under vacuum at room temperature for 24 h to remove all the volatiles. Finally, the plates were cured at 100 °C for 1 h into a furnace. Carbon dot reduced Cu_2O nanohybrid/hyperbranched epoxy nanocomposites were coded as ECDCO0.5, ECDCO1.0 and ECDCO1.5, respectively.

5A.2.3.3. Photocatalytic activity

Photodegradation of ethyl paraoxon organophosphate pesticide was chosen for the determination of photocatalytic activity of the nanocomposites. In a typical procedure, 10 × 10 × 0.3 mm^3 size (average weight 0.1-0.12 g) film of ECD1.0 (hyperbranched epoxy nanocomposite with 1 wt% carbon dot as reported in sub-chapter 4B, used for comparison purpose) and ECDCO1.0 nanocomposites was cut into a few small pieces and taken in 25 mL aqueous solution of pesticide (10 ppm) separately. The solutions were stirred in the presence of above small pieces of nanocomposites under normal solar light (not directly under sunlight, light intensity: 800-1000 lux) at room temperature (25 °C). The experiment was also done for carbon dot reduced Cu_2O nanohybrid at same amount of active agent (1 wt%, 0.001g) for the comparison purpose. The change in concentration of the pesticide was monitored by detecting UV absorbance intensity at wavelength 300 nm for specified time

intervals. The activity of the catalyst is calculated from the rate of change of concentration of pesticide. On complete degradation of pesticide, the pieces of catalysts were taken out by normal filtration and weight was taken after drying at room temperature. These used catalysts were further recycled to examine its reusability.

5A.3. Results and discussion

5A.3.1. Preparation and characterization of carbon dot reduced Cu_2O nanohybrid

Carbon dot reduced Cu_2O nanohybrid was prepared by reduction of Cu^{2+} by carbon dot. In this reduction process, carbon dot not only acts as reducing agent, but it also helps as a capping agent. This is because of the fact that a large number hydroxyl, carbonyl, carboxylic acid and epoxy groups are present on the surface of carbon dot, as reported in sub-chapter 4A. Mainly peripheral polar groups like hydroxyl and aldehyde of carbon dot help to reduce the Cu^{2+} into Cu^{+}. The hydroxyl groups reduce Cu^{2+} by polyphenolic mechanism; on the other hand the aldehyde groups reduce Cu^{2+} like Benedict reaction as shown in **Scheme 5A.1**. In FTIR spectra (**Figure 5A.1**) it was found that the amount of hydroxyl groups (at 3400-3500 cm^{-1}) of carbon dot decreased after formation of carbon dot reduced Cu_2O nanohybrid, whereas the amount of carbonyl groups (at 1650 cm^{-1}) was increased. This is because of the fact that the hydroxyl groups are converted into keto groups, while aldehyde groups are converted into carboxylic acid groups. Other functional groups and chemical linkages of carbon dot remained intact after formation of nanohybrid. The Cu-O bonds were found in FTIR spectrum of nanohybrid at 465 and 556 cm^{-1}. The peripheral polar groups of carbon dot also stabilize Cu_2O nanoparticles. In optical absorption spectrum of nanohybrid (**Figure 5A.2a**), the π-π^* and n-π^* transitions of carbon dot were found at 240 and 275 nm, while the absorption peak for Cu_2O nanoparticle was appeared at around 500-600 nm. The formation of nanohybrid was confirmed by TEM study (**Figure 5A.3**). **Figure 5A.3a** reveals that the nanoparticles are nearly spherical in shape with average diameter of around 3-4 nm. From **Figure 5A.3a** and **5A.3b**, it was confirmed that Cu_2O attached carbon dot and carbon dot embedded Cu_2O were formed. The formation of Cu_2O was confirmed from XRD pattern of the nanohybrid (**Figure 5A.4**). From this figure, the peaks at 2θ (°) = 36.4, 42.3, 61.4 and 73.5 correspond to crystallographic spacing d_{111}, d_{200}, d_{220} and d_{311}, respectively for Cu_2O nanoparticles were found in accordance to other reports and JCPDS 78-2076 data.[22-24] Bright spots in SAED pattern (**Figure 5A.3d**) of TEM analysis also confirmed the presence of Cu_2O crystals. Carbon dot possesses amorphous or poor crystalline structure as reported in sub-chapter 4A. Two types of lattice spacing, d_{111} spacing of Cu_2O (0.27 nm) and d_{002} (0.38 nm)

spacing of carbon dot were found as shown in inset picture of TEM images (**Figure 5A.3a** and **5A.3b**).[8]

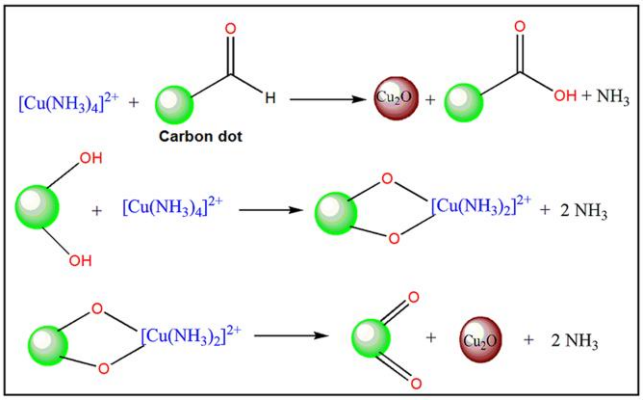

Scheme 5A.1: Reduction mechanism for the preparation of carbon dot reduced Cu_2O nanohybrid

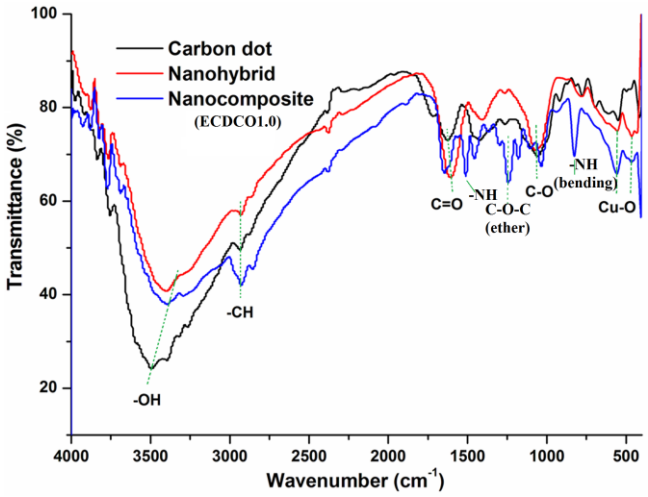

Figure 5A.1: FTIR spectra of carbon dot, carbon dot reduced Cu_2O nanohybrid and ECDCO1.0

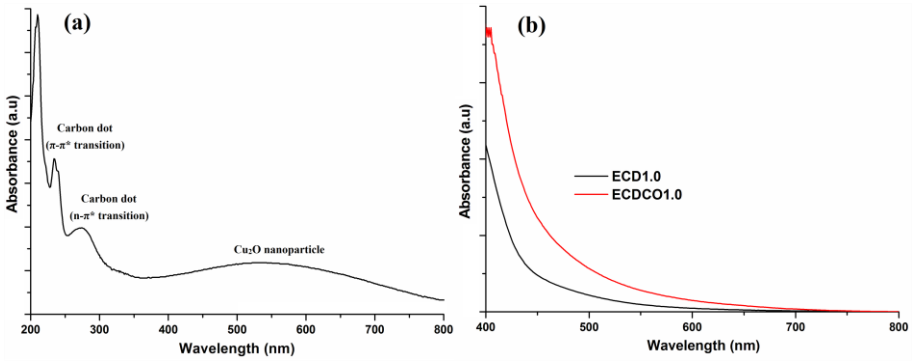

Figure 5A.2: Optical absorption spectra of (a) carbon dot reduced Cu_2O nanohybrid and (b) ECD1.0 and ECDCO1.0

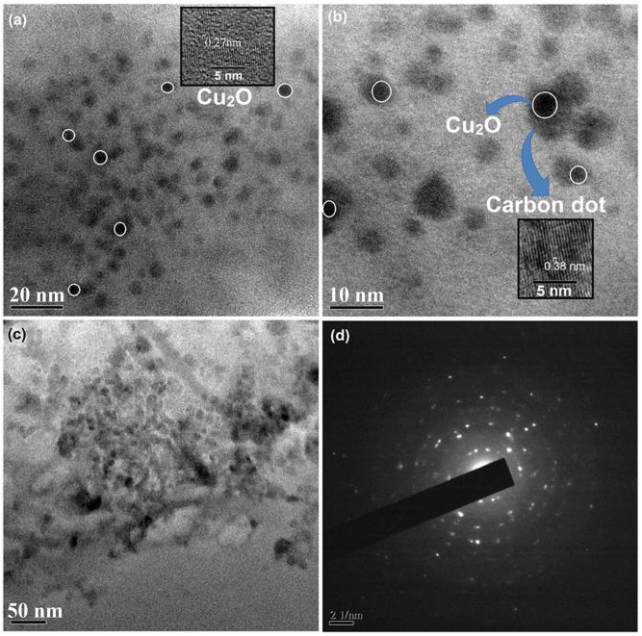

Figure 5A.3:TEM images: (a) high magnification (inset: the internal structure of Cu_2O), (b) low magnification (inset: the internal structure of carbon dot) of carbon dot reduced Cu_2O nanohybrid, (c) TEM image of ECDCO1.0 and (d) selected area electron diffraction (SAED) pattern of carbon dot reduced Cu_2O nanohybrid

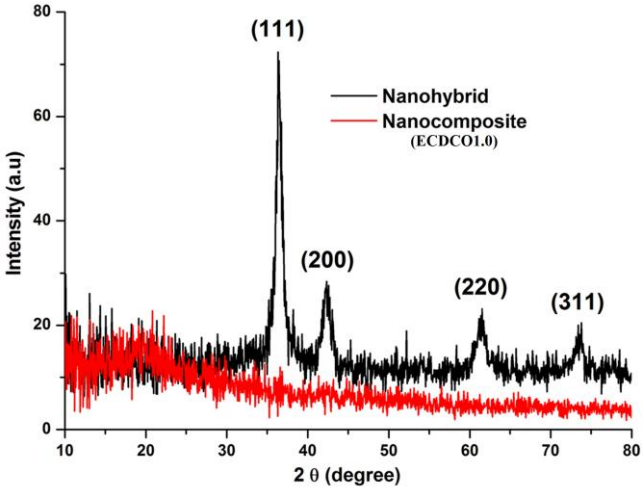

Figure 5A.4: XRD patterns for carbon dot reduced Cu_2O nanohybrid and ECDCO1.0

5A.3.2. Preparation and characterization of nanocomposites

Nanocomposites were prepared by solution technique and cured with PAA hardener. The hyperbranched epoxy nanocomposite with 1 wt% of carbon dot (ECD1.0) was used here only for comparison purpose and it was already characterized in sub-chapter 4B. The representative carbon dot reduced Cu_2O nanohybrid/hyperbranched epoxy nanocomposite

(ECDCO1.0) was characterized by FTIR, XRD and TEM analyses. In FTIR spectra (**Figure 5A.1**) the hydroxyl band of carbon dot reduced Cu_2O nanohybrid shifted to 3390 from 3415 cm^{-1} after formation of nanocomposite. This is due to the presence of different physico-chemical interactions of carbon dot and Cu_2O nanoparticles with hyperbranched epoxy. Due to the same reason, the Cu-O bands of nanohybrid also shifted to 558 and 468 cm^{-1} after formation of nanocomposite. The other strong bands around 1500 and 800 cm^{-1} are due to the –NH stretching and bending vibration for PAA hardener, respectively. Ether linkage for hyperbranched epoxy and carbon dot is assigned at 1250 cm^{-1}. The strong interaction of nanoparticles with hyperbranched epoxy matrix was also revealed from XRD patterns (**Figure 5A.4**). The crystallographic peaks of nanohybrid were completely diminished after formation of nanocomposite, whereas an amorphous polymeric peak at $2\theta = 20°$ was observed. The diminished of Cu_2O peaks may also due to the masking effect by the polymer matrix (as the amount of Cu_2O is very low compared to the matrix). Good dispersion and interaction of nanohybrid with the matrix was confirmed in TEM image (**Figure 5A.3c**) of carbon dot reduced Cu_2O nanohybrid/hyperbranched epoxy nanocomposite. The optical absorption spectra of ECDCO1.0 and ECD1.0 films are given in **Figure 5A.2b**. From the spectra, it was found that ECDCO1.0 film absorb more visible light than ECD1.0 film due to combine absorption of visible light by carbon dot and Cu_2O nanoparticles.

5A.3.3. Mechanical properties of the nanocomposites

The results of mechanical properties like tensile strength, elongation at break, toughness, impact resistance, scratch hardness and bending values of pristine hyperbranched epoxy and nanocomposites are given in **Table 5A.1**. From the results, it was found that tensile strength of pristine epoxy was improved up to 20% after formation of nanocomposite with 1.5 wt% nanohybrid. However, elongation at break and toughness of hyperbranched epoxy thermoset was increased dramatically by factors 2.5 and 3.5 folds after formation of nanocomposite with the same amount of nanohybrid. The stress-strain profiles of the nanocomposites are shown in **Figure 5A.5**. From the figure, it can be found that tensile strength, elongation at break and toughness (area under stress-strain curves) of the hyperbranched epoxy thermoset increased with the increase of amount of nanohybrid loading. The simultaneous improvement in strength, elasticity and toughness is due to strong physico-chemical interactions of the matrix with the quantum size carbon dot as described in sub-chapter 4B. The presence of carbonized aromatic structure of carbon dot enhances the strength of nanocomposite and the peripheral polar functional groups of carbon dot provide strong physico-chemical interactions

with the hyperbranched epoxy and PAA, which simultaneously increase the elasticity and toughness of nanocomposites as observed in sub-chapter 4B. Very small size of carbon dot and Cu_2O nanoparticles also provide large surface area for strong interactions with the matrix, which enhance all the mechanical properties of nanocomposites. As toughness of hyperbranched epoxy thermoset was dramatically improved, the other mechanical properties like impact resistance and scratch hardness which were related to toughness were also improved by the formation of nanocomposites. However, these differences could not be measured as the values for nanocomposites reached the highest limit of the instruments for scratch hardness (10 kg) and impact resistance (100 cm). Nanocomposites were also exhibited the highest limit of the instrument for the flexibility evaluation (1 mm bending diameter of mandrel) without any damage of the film.

Table 5A.1: Performance of pristine hyperbranched epoxy (TAHE20) and its nanocomposites with carbon dot and carbon dot reduced Cu_2O nanohybrid

Parameter	TAHE20*	ECDCO0.5	ECDCO1	ECDCO1.5
Swelling value (%)	24±0.2	24±0.4	23±0.3	21±0.2
Tensile strength (MPa)	40±1	43±1.5	45±1	48.5±1.5
Elongation at break (%)	21±1	28.5±3	40±2	49.5±2
Toughness (MPa)	540	874	1370	1868.5
Scratch hardness (kg)	9.0	>10.0	>10.0	>10.0
Impact resistance (cm)	>100	>100	>100	>100
Bending diameter (mm)	<1	<1	<1	<1
Initial degradation temperature (°C)	267	286	287	296

*As reported in sub-chapter 2B

5A.3.4. Thermal stability of the nanocomposites

Initial degradation temperatures of pristine hyperbranched epoxy and its nanocomposites are given in **Table 5A.1** and TGA curves are shown in **Figure 5A.6**. From the results, it was found that the initial degradation temperature of hyperbranched epoxy thermoset increased up to 29 °C after formation of nanocomposite with 1.5 wt% nanohybrid. The initial degradation temperature increased with the increase of amount of nanohybrid loading. The improvement in thermal stability is due to the strong interactions of quantum size carbon dot and Cu_2O

nanoparticles with hyperbranched epoxy and PAA. The quantum size of carbon dot and Cu_2O nanoparticles provide large surface area for strong interactions. Again, the presence of carbonized aromatic structure and peripheral polar functional groups of carbon dot provide strong physico-chemical interactions with the matrix, which also enhances the thermal stability of nanocomposites. In addition to that, nanohybrid acts as mass transport barrier to the volatile products generated during decomposition by providing longer paths for them to travel.[25]

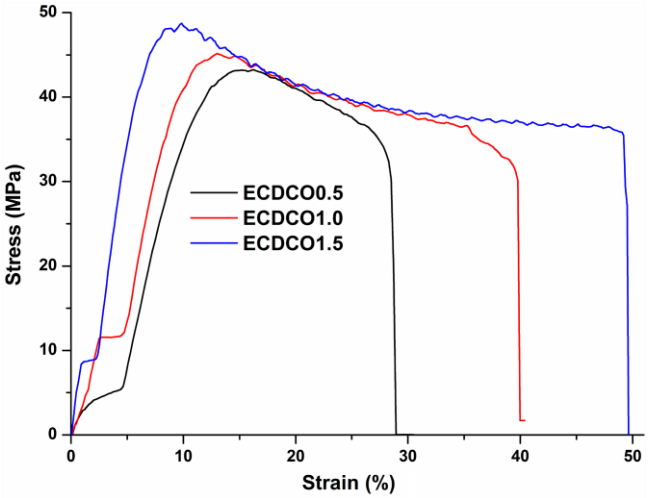

Figure 5A.5: Stress-strain profiles of the nanocomposites

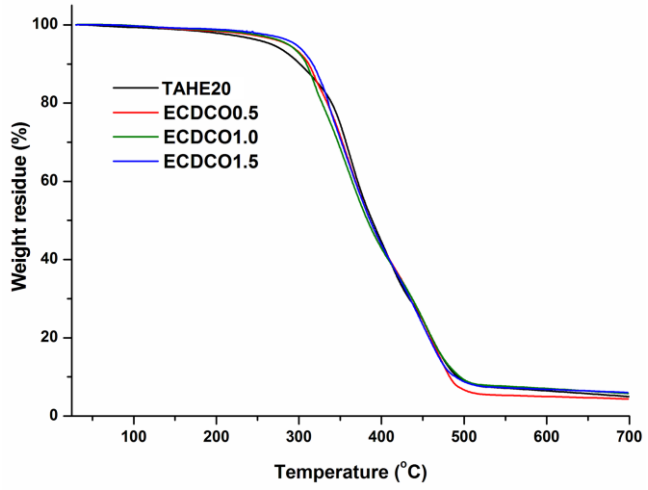

Figure 5A.6: TGA thermograms for pristine thermoset and its nanocomposites with nanohybrid

5A.3.5. Photocatalytic activity

Photocatalytic degradation of paraoxon pesticide was studied by ECDCO1.0 and ECD1.0 nanocomposite films under normal solar light (not directly exposed under the sunlight). The nanocomposite film was chopped into small pieces to increase the surface area as well as to expose the Cu_2O nanoparticles. The concentration changes of the pesticide with time were monitored by UV absorbance. The plots of optical absorbance against wavelength for the degradation of pesticide at different times for both ECDCO1.0 and ECD1.0 are shown in **Figure 5A.7a** and **5A.7b**, respectively. The rate of degradation of pesticide with time for ECDCO1.0 (both in dark and solar light), ECD1.0 and nanohybrid is shown in **Figure 5A.7c**. From these figures, it is clear that the time taken for 90% degradation of the pesticide was 5 h by ECDCO1.0 film, whereas only 50% degradation of the same by ECD1.0 film was observed after 12 h under solar light, whereas no degradation was observed under dark. In case of photocatalytic activity of nanohybrid, the initial degradation rate of the nanohybrid is slightly slower than the nanocomposite film. This may be due to the presence of different polar functional groups of hyperbranched epoxy, which may interact with the polar organophosphate pesticide and adhere on its surface. This facilitates the interaction with the active oxygen radicals. However, as same amount of active agent (1 wt% nanohybrid) was used in both the cases, so the same extent of degradation was observed under the same total period of exposure. On the other hand, the recovery of the nanohybrid catalyst is difficult due to its nano level dispersion in water by strong interactions of polar functional groups of carbon dot. The recovery of this catalyst needs large amount of organic solvent (acetone) as well as high speed in centrifugation (8000-10000 rpm) process. On the other hand, the nanocomposite film can be easily recovered from the reaction medium (water). However, the activity of pure commercial Cu_2O nanoparticles was reported in literature for photocatalytic degradation of dye and found <3% of dye degradation.[8] Literature also reported the degradation of the pesticide using different nanophotocatalysts,[14] but in all the cases the photocatalytic activity was studied under UV irradiation. Further, the efficiency of these catalysts is inferior compared to the presently reported catalyst, where there is no need of any additional energy other than normal solar light.

The pseudo-first order kinetic model equation was used to describe the photo-degradation behavior of nanocomposite films. The equation used is

$$-dC/dt = K_1 t \quad \text{(5A.1)}$$

where, C is the concentration of pesticide at any time t and K_1 is the apparent rate constant. After integrating the equation (5A.1), the following equation is obtained

$$\ln(C/C_0) = -K_1 t \quad \text{(5A.2)}$$

where, C_0 is the initial concentration (at t = 0) of pesticide. The fitting plots of $\ln(C/C_0)$ versus time are shown in **Figure 5A.7d** and demonstrate that the degradations of paraoxon pesticide is well described by pseudo-first order kinetics with the fitting coefficients over 0.9, indicating regular photo-degradation behavior.[7]

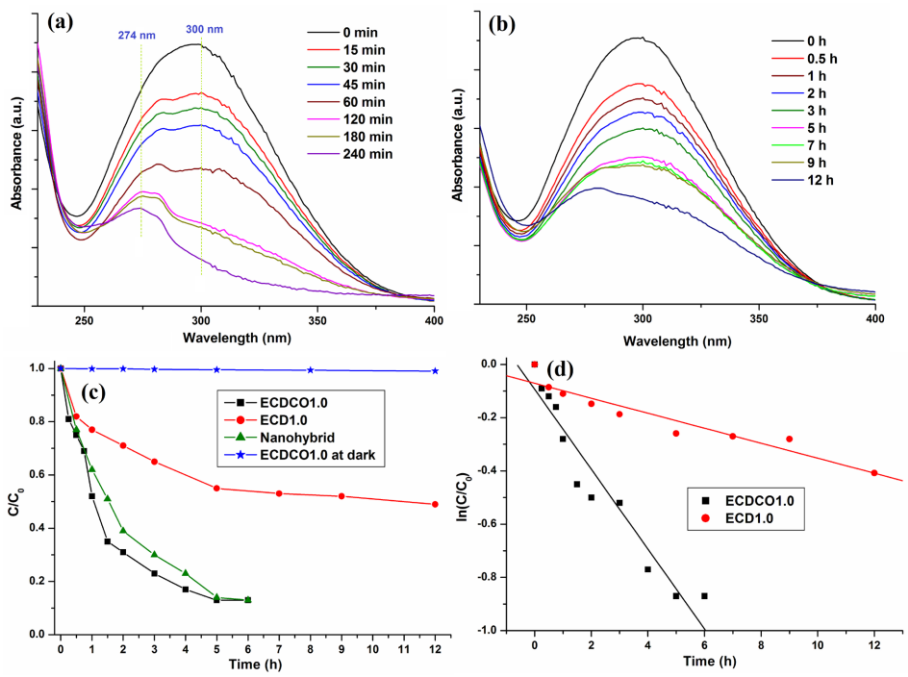

Figure 5A.7: Plots of UV absorbance against wavelength at different times for degradation of paraoxon pesticide in the presence of (a) ECDCO1.0 and (b) ECD1.0 film, (c) plots of degradation rate for ECDCO1.0 (at dark and solar light), ECD1.0, nanohybrid; and (d) fitting curves for the ECDCO1.0 and ECD1.0 for pseudo-first order model

Photodegradation mechanism is schematically illustrated in **Scheme 5A.2** based on other reported carbon dot/metal or metal oxide nanoparticles by exploiting the up-conversion luminescence properties of carbon dot.[8,20,21] When ECDCO1.0 nanocomposite film was exposed under solar light with the pesticide solution, carbon dot absorbs visible light as well as near infrared light and emits shorter wavelength of light (300-500 nm). This shorter wavelength of light again excites Cu_2O nanoparticles and form electron/hole (e^-/h^+) pairs. These e^-/h^+ pairs react with H_2O and O_2 to produce active oxygen radicals like $^{\cdot}OH$, $^{\cdot}O_2^-$ which take part in the degradation of paraoxon pesticide. In case of ECD1.0 nanocomposite only $^{\cdot}O_2^-$ radicals are formed, and thus degradation of pesticide is taken place at relatively slow rate.[8,20,21] ECDCO1.0 also absorb more visible light compared to the ECD1.0 as revealed from absorption spectra (**Figure 5A.2b**), which helps to increase the catalytic

efficiency of ECDCO1.0 under solar light. The products form after degradation of the pesticide are H_2O, CO_2, phosphoric acid, N_2, O_2 etc. as reported in literatures.[13,14]

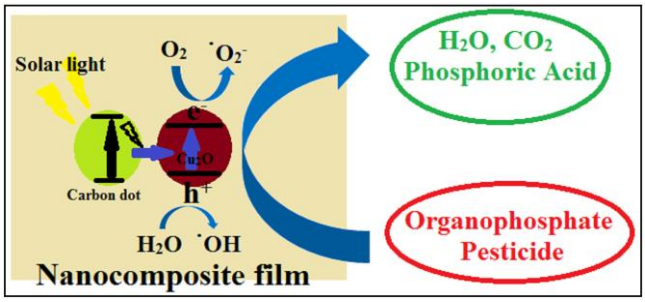

Scheme 5A.2: Photocatalytic mechanism for nanocomposite film

The catalytic activity of the reused photocatalyst was checked up to third cycle and the results are given in **Table 5A.2**. The catalytic activity as well as the weight of the nanocomposite films remained almost constant. This is because of the strong interaction of nanoparticles with hyperbranched epoxy and PAA, and thus no leaching of materials was taking place. In case of ECD1.0, a negligible weight loss (0.1-0.2%) and thus loss of catalytic activity of the films was observed after 3rd cycle, which may be due to long exposure time of the film in the pesticide solution.

Table 5A.2: Catalytic activity at different cycles of reuse

Catalyst	No. of cycle	Degradation time (h)	Percentage of degradation	Weight loss (%)
ECDCO1.0	1st	5	90	0
	2nd	5	90	0
	3rd	5	90	0
ECD1.0	1st	12	50	0
	2nd	12	50	0.11
	3rd	12.25	50	0.17

5A.4. Conclusion

So in this study, we demonstrated a high performance thermostable hyperbranched epoxy nanocomposite, which exhibited potocatalytic activity towards degradation of a health

hazardous pesticide under solar light. Carbon dot reduced Cu_2O nanohybrid was successfully prepared *in-situ* by simple reduction of cupric acetate solution by carbon dot. Hyperbranched epoxy thermoset acted as a very good polymeric support for efficient recycling and reuse of the catalyst by providing strong physico-chemical interactions with the nanohybrid.

5B. Hyperbranched epoxy/biocide immobilized OMMT-carbon dot reduced Cu_2O nanocomposites

5B.1. Introduction

The importance of antimicrobial polymer nanocomposites was mentioned in sub-chapter 3B. In recent years, antimicrobial materials are gaining strong impetus for the prevention of infection, water purification, marine coating, etc. In this milieu, inorganic nanoparticles and organic biocides are considered as effective antimicrobial agents.[26-29] However, direct use of thermo-labile organic biocide as an antimicrobial agent may cause risk to human health and environmental hazard.[27] Although copper based inorganic nanomaterials possess strong inhibitory/killing effect to different microorganisms,[30-33] but they also suffer from some practical drawbacks. First of all, metallic Cu nanoparticles are highly toxic to higher animals too.[27] Further, formation and stabilization of Cu nanoparticles are also challenging issues. On contrary, Cu_2O nanoparticles are nontoxic to higher animals, easily available and relatively cheap as described in previous sub-chapter. Further, they act as p-type semiconductor with a band gap 2.2 eV, which may be explored to generate active free radicals to kill or inhibit the microorganisms under suitable conditions.[7,16] However, Cu_2O nanoparticles are not used frequently as antibacterial agent,[34,35] because of their low activity, particularly against fungus or algae. Further as mentioned previously, controlled reduction of Cu^{2+} to produce Cu_2O nanoparticles is difficult. Whereas, carbon dot reduced Cu_2O nanohybrid can easily produced in a controlled manner as observed in sub-chapter 5A. Moreover, carbon dot has tunable emissions from near-infrared to blue wavelength and it exhibits unique up-conversion photoluminescence property as stated in sub-chapter 5A. Thus, carbon dot can generate electron/hole (e^-/h^+) pairs by the excitation of semiconductor metal oxide nanoparticles like Cu_2O, TiO_2, etc. as reported in literature as well as described in previous sub-chapter.[8,20,21] These e^-/h^+ pairs react with H_2O and O_2 to produce active oxygen radicals like $^{\cdot}OH$, $^{\cdot}O_2^-$ which may also help in killing the microorganisms. However, bare nanoparticles cannot be used as antimicrobial agents for long duration as they lose their stability and functions due to agglomeration. In this milieu, fabrication of nanocomposite of the metal nanoparticles with polymer or immobilization of the organic biocides into such polymer nanocomposites is an advanced technique for the destruction of microorganisms by slow release of the active agents.[36,37] This technique reduces the toxic effect of the active agents to the environment as well as provides stability to the same with long durability. Again, stable and homogenous dispersions of metal nanoparticles are achieved by using polymer supported organo-modified

clay templated system. The resultant nanocomposite also offers excellent mechanical performance to the pristine system as observed in Chapter 3. This organo-modified clay has layer structure with high aspect ratio, which allows efficient load tolerance to the polymer matrix, and thus provides high strength and stiffness to the nanocomposite.[38,39] Further, clay is also inherently nontoxic and has the capacity to absorb inorganic and organic molecules.[27] Thus, unison of inorganic nanoparticle and organic biocide may result in an advanced antimicrobial agent with enhanced activity to address a spectrum of microorganisms with different characters.[26,27]

In the present sub-chapter, therefore, a biocide immobilized OMMT-carbon dot reduced Cu_2O nanohybrid/hyperbranched epoxy nanocomposite was investigated as a high performance advanced antimicrobial material with photoluminescence attribute.

5B.2. Experimental

5B.2.1. Materials

Hyperbranched epoxy (TAHE20) and carbon dot reduced Cu_2O nanohybrid related materials are same as reported in the previous sub-chapter. OMMT nanoclay was also same as used in sub-chapter 3B. Here, only 2-methyl-4-isothiazolin-3-one hydrochloride (MITH) was immobilized for achieving significant antimicrobial activity as it is a powerful synthetic biocide.[40] It was purchased from Sigma Aldrich, Germany.

5B.2.2. Characterization

The instrumentation and characterization techniques for spectroscopic, microscopic, XRD, mechanical, thermal testing were same as reported previous chapters.

5B.2.3. Methods

5B.2.3.1. Preparation of OMMT-carbon dot Cu_2O nanohybrid

OMMT-carbon dot reduced Cu_2O nanohybrid was prepared by reduction of $Cu(OAc)_2$ solution using carbon dot in the presence of OMMT. First, copper-ammonium complex was prepared by the same procedure as mentioned in the previous sub-chapter. In a typical process, 0.5 g $Cu(OAc)_2$ was dissolved in 25 mL EtOH by stirring for 15 min in a two necked round bottom flask. An amount of 20 mL aqueous solution of NH_3 (30%) was added to the solution and stirred for another 15 min at room temperature. Then, an amount of 1.0 g of OMMT was dispersed in 50 mL EtOH by stirring for 30 min in a 100 mL reagent bottle and it was added drop wise to the above copper-ammonium complex under constant stirring at

room temperature. After 1 h, the round bottom flask was equipped with a water condenser and the temperature was raised to 70 °C. Then, a 25 mL ethanolic carbon dot solution (0.5 g) was added drop wise to the mixture and stirred for 6 h. After completion of the reaction, the solution was cooled down naturally and separation of the nanohybrid particles was done by ultracentrifugation at 5000 rpm for 10 min. The nanohybrid particles were washed with EtOH for 2-3 times and finally dispersed in 20 mL THF by ultrasonication for 5 min as stated in the previous sub-chapter. The prepared nanohybrid was coded as ECDCONC.

5B.2.3.2. Immobilization of biocide

MITH was immobilized on ECDCONC by combined effect of mechanical shearing and ultrasonic forces at room temperature. In a typical process, 0.5 g ECDCONC was dispersed in 25 mL THF under constant stirring for 30 min in a 60 mL glass bottle. An amount of 20 wt% of MITH (0.1 g) with respect to ECDCONC nanohybrid was added to it and stirred continuously for 2 h at room temperature followed by ultrasonication for 10 min. MITH immobilized nanohybrid was coded as MITH-NH.

5B.2.3.3. Preparation of hyperbranched epoxy nanocomposites with MITH-NH

The hyperbranched epoxy nanocomposites with different amount of MITH-NH (1, 2 and 3 wt% MITH-NH containing biocide: 0.2, 0.4 and 0.6 wt% with respect to hyperbranched epoxy) were prepared by solution technique as described in the previous sub-chapter. The requisite amount of the THF dispersed nanohybrid particles were added to the hyperbranched epoxy resin and stirred magnetically for 2h at room temperature followed by ultrasonication for 10 min. The nanocomposite films were prepared by similar way as described in the previous sub-chapter and cured with 50 wt% of PAA hardener at 100 °C for 1h followed by post curing at 130 °C for 30 min. The nanocomposites were coded as MITH-NH1, MITH-NH2 and MITH-NH3 for 1, 2 and 3 wt% of MITH-NH respectively. The hyperbranched epoxy nanocomposites with 1, 2 and 3 wt% ECDCONC nanohybrid (without immobilization of biocide) separately, were only used in antimicrobial study for comparison purpose and are coded as ECDCONC1, ECDCONC2 and ECDCONC3 respectively.

5B.2.3.4. Antimicrobial and biofilm formation study

Antimicrobial and biofilm formation studies were performed by same methods as described in sub-chapter 3B.

5B.3. Results and discussion

5B.3.1. Formation and characterization of nanohybrid

OMMT-carbon dot reduced Cu_2O nanohybrid was prepared in a single pot by reduction of $Cu(OAc)_2$ solution by carbon dot in presence of OMMT. The reduction mechanism is same as shown in the previous sub-chapter (**Scheme 5A.1**). Here, OMMT acts as a stabilizer for carbon dot as well as Cu_2O nanoparticles by absorbing them on its surface and inside the platelets (**Scheme 5B.1**). From TEM images of ECDCONC (**Figure 5B.1a** and **5B.1b**), it can be seen that the small tiny particles of carbon dot and Cu_2O are attached on the surface as well as inside the platelets of OMMT. Carbon dot contain large numbers of polar functional groups on its surface, which may cause to coalesce by the intermolecular attractions. Again, nanomaterial possesses high surface area with extremely large numbers of surface atom compared to interior, which results high surface energy. To minimize this surface energy nanomaterial is aggregated if the same is not stabilized by steric or electrostatic stabilizer. However, in presence of OMMT, these groups help to interact with the polar groups of the OMMT platelets by different polar-polar interactions and thus nanoparticles are stabilized on the surface of OMMT. Here, from the TEM images, two types of lattice spacing of 0.27 and 0.36 nm were found, which correspond to the d_{111} spacing of Cu_2O and d_{002} spacing of carbon dot, respectively as shown in **Figure 5B.1c**.[8] The formation of Cu_2O was confirmed from the XRD study. In the XRD pattern (**Figure 5B.2**) of ECDCONC the same crystallographic spacing of carbon dot reduced Cu_2O nanohybrid were found along with d_{001} and d_{002} peaks at 2θ (°) = 7.08 and 19.82 respectively for OMMT crystal. However, in this case the intensity of Cu_2O peaks were very low due to the absorption of Cu_2O nanoparticles into the OMMT platelets as well as masking effect by OMMT as amount is higher than Cu_2O. Again, after immobilization of MITH the d_{001} crystallographic peak of OMMT was shifted from 2θ (°) = 7.08 to 5.45. Thus, the interlayer spacing of OMMT increases from 1.2 to 1.6 nm after immobilization of MITH. This increase of interlayer spacing is due to the combining effect of mechanical shearing and ultrasonication forces, which help in dispersion of OMMT and interactions of its layers with MITH by the presence of polar groups in both. The ultrasonication and mechanical shearing forces also help to interact MITH with the surface of carbon dot and Cu_2O nanoparticles. The polar functional groups of carbon dot and quantum size of both carbon dot and Cu_2O nanoparticles strengthen the interactions with MITH molecules. MITH is immobilized under ambient condition. Even though biocide is stored at low temperature but on immobilization, its storage stability is enhanced. The biocide is adsorbed immediately on the surface of the nanohybrid, because of high surface area and

surface energy and thereby gaining the stability with retaining activity. Literature supports similar observation for nanomaterial immobilized enzyme.[41]

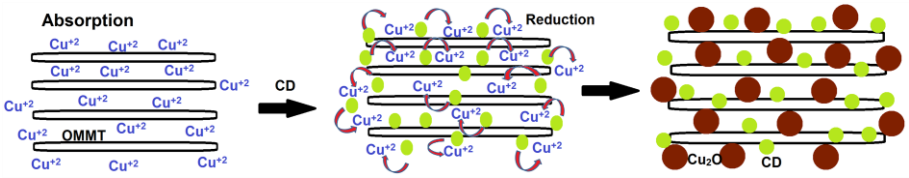

Scheme 5B.1: Formation of ECDCONC

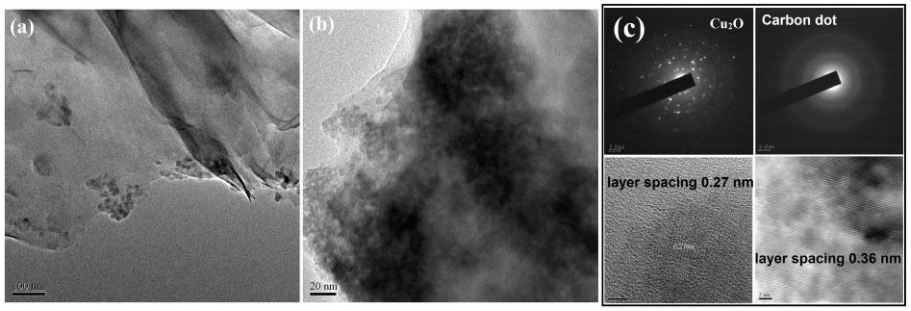

Figure 5B.1: TEM images of ECDCONC at (a) 100 nm and (b) 20 nm resolutions; and (c) SAED patterns of Cu_2O, carbon dot and their interlayer spacings obtained from TEM images

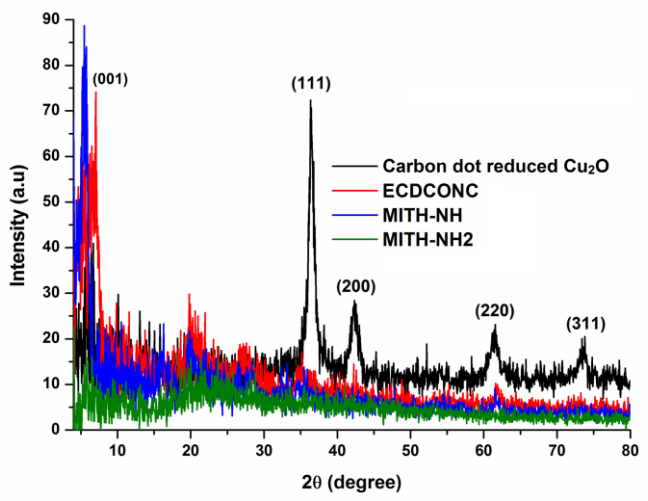

Figure 5B.2: XRD patterns of nanohybrids and MITH-NH2 nanocomposite

5B.3.2. Preparation and characterization of nanocomposites

Hyperbranched epoxy nanocomposites with 1, 2 and 3 wt% of MITH-NH were prepared by solution technique with the help of combined effect of mechanical shearing and ultrasonic forces. Mechanical shearing helps to mix the matrix and nanohybrid homogeneously,

whereas ultrasonication generates small cavities in the liquid medium by mechanical vibrations with high frequency. These cavities rapidly create microscopic shock waves. This cavitation is extremely powerful when all the imploding cavities are combined. Such cavities are formed and collapsed within microseconds, thereby releasing tremendous energy within the liquid medium.[42] This energy is utilized to disperse the nanohybrid and OMMT in hyperbranched epoxy matrix. Thus, the use of ultrasonication force prevents the agglomeration of the nanohybrid by strong interactions of the OMMT layers, carbon dot and Cu_2O nanoparticles with hyperbranched epoxy matrix during the preparation of nanocomposites. These forces therefore, help the OMMT platelets to interact with hyperbranched epoxy and hence well dispersed platelets into the matrix were obtained. As a result, d_{001} peak in XRD analysis ($2\theta = 5.45°$) was completely vanished after formation of nanocomposite as found in **Figure 5B.2**. The direct visualization of well dispersed OMMT platelets as well as carbon dot reduced Cu_2O nanohybrid particles were found in TEM images (**Figure 5B.3**) of nanocomposite. The well dispersed and disordered arrangement of clay layers inside the hyperbranched epoxy matrix was found in **Figure 5B.3a** and **5B. 3c**. The dispersion of the OMMT platelets and the carbon dot reduced Cu_2O nanohybrid particles are shown in **Figure 5B.3b**, where the carbon dot reduced Cu_2O nanohybrid particles are attached with the OMMT surface and well-separated from each other without aggregation. This is due to the strong physico-chemical interactions between the polar functional groups of matrix, nanohybrid particles (mainly OMMT platelets and carbon dot) and MITH. In **Figure 5B.3d**, the intercalation behavior of OMMT platelets by the matrix was found. The interlayer spacing between the OMMT platelets was found to be ~1.3 nm as shown in **Figure 5B.3d**. This is because of the hyperbranched epoxy chains intercalate the clay galleries by the strong interactions with the OMMT platelets assisted by immobilized MITH.

The percentage of swelling values of the cured nanocomposites and the pristine thermoset are given in **Table 5B.1**. The swelling values of the nanocomposites decrease with the increase of amount of nanohybrid loading, and thus the extent of crosslinking is increased. This is due to the fact that the nanohybrid particles act both as physical and chemical crosslinkers with the hyperbranched epoxy as well as PAA hardener as reported in Chapter 4. Here, polar functional groups of carbon dot can chemically react with hyperbranched epoxy and PAA hardener as shown in sub-chapter 4B. OMMT can also act as a chemical crosslinker and assisted by polar groups of immobilized MITH.

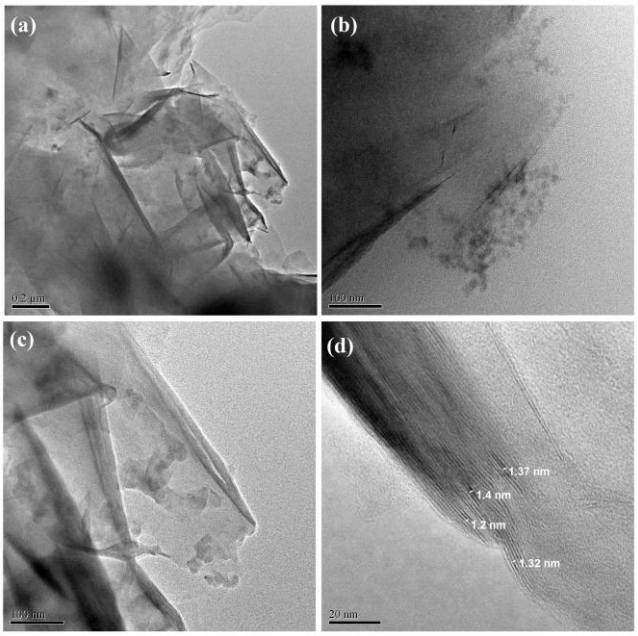

Figure 5B.3: TEM images of MITH-NH2 at different resolutions and positions: (a) at 0.2 μm, (b) 100 nm, (c) 100 nm at different position and (d) OMMT layer spacing at 20 nm resolution

5B.3.3. Mechanical properties of nanocomposites

The values of mechanical properties for the nanocomposites and the pristine thermoset are given in **Table 5B.1**. Tensile strength, elongation at break and toughness values of the pristine hyperbranched epoxy thermoset sharply increased after formation of nanocomposites with MITH-NH. The tensile strength of pristine thermoset increased from 40 to 72.5 MPa after formation of MITH-NH3. From the stress-strain profiles (**Figure 5B.4**), it is found that elongation at break and toughness (area under stress-strain curve) of pristine thermoset were dramatically improved after formation of nanocomposites with MITH-NH. A 3 fold increment in elongation at break and 4 fold increment in toughness of the pristine system were observed for MITH-NH3. The improvement in tensile strength may be due to chemical crosslinking of peripheral polar functional groups of carbonized aromatic carbon dot and polar groups of immobilized MITH-OMMT with hyperbranched epoxy and PAA as mentioned in the earlier chapters. The strong physical interactions among partially exfoliated OMMT platelets, quantum size carbon dot and Cu_2O nanoparticles with the polymer matrix also increase the tensile strength. Dramatic enhancement in elongation at break and toughness is due to the physical crosslinking of the nanoparticles with hyperbranched epoxy and plasticizing effect of PAA. The mobility of partially exfoliated OMMT platelets assisted by the immobilized MITH as well as spherical carbon dot and Cu_2O nanoparticles inside the clay

galleries also provides a mode of energy dissipation. The different flexible moieties like aliphatic hydrocarbon, ether, etc. of hyperbranched epoxy and PAA increase both strain and toughness of the material by plasticizing effect as stated earlier. However, in case of hyperbranched epoxy nanocomposite with 1 wt% only carbon dot reduced Cu_2O nanohybrid ECDCO1.0 in previous sub-chapter, only 12.5% improvement in tensile strength was occurred though improvements in elongation at break and toughness were more than 2 fold. The improvements in scratch hardness and impact resistance could not be measured, as the values for the nanocomposites have reached the highest limit of the instruments for scratch hardness (10 kg) and impact resistance (100 cm) as given in **Table 5B.1**. The nanocomposites also exhibited the lowest limit of the instruments for the flexibility evaluation (bending diameter of mandrel is 1 mm) as they possessed high elongation at break.

5B.3.4. Thermal stability of nanocomposites

The initial thermal degradation (5% weight loss) temperatures of the pristine thermoset and its nanocomposites are given in **Table 5B.1** and TGA curves are shown in **Figure 5B.5**. From the results, it was found that the initial degradation temperature of hyperbranched epoxy thermoset increased up to ~30 °C after formation of nanocomposite with 3 wt% MITH-NH nanohybrid. The initial degradation temperature increased with the increase in the amount of nanohybrid loading. This improvement in thermal stability is due to the strong interactions of the quantum sizes carbon dot and Cu_2O nanoparticles with hyperbranched epoxy and PAA, as stated earlier. The quantum sizes of carbon dot and Cu_2O nanoparticles provide large surface area for such strong interactions as mentioned in the previous sub-chapter. Moreover, the presence of carbonized aromatic structure and peripheral polar functional groups of carbon dot provide strong physico-chemical interactions with the matrix, which also enhance the thermal stability of nanocomposites as seen in the sub-chapter 5A. Another reason for increase in thermal stability of pristine thermoset after formation of nanocomposites is due to the intercalation of OMMT clay galleries by hyperbranched epoxy and PAA chains, which restricted the segmental motion of the polymer chains by different physico-chemical interactions. In addition to the above, the improvement in initial decomposition temperature of the nanocomposite by incorporation of OMMT is due to the fact that clay is a heat insulator and acts as a mass transport barrier to the volatile products generated during decomposition by providing long paths for them to travel as described in sub-chapter 3B as well as in literature.[25] Both pristine thermoset and nanocomposites were degraded mainly by two stage patterns in TGA curves (**Figure 5B.5**), where the first step (~300 °C) is related to

the degradation of aliphatic moieties and the second stage (~400 °C) is due to degradation of aromatic moieties as noticed earlier also. However, in case of ECDCO1.0 only 20 °C improvement in initial degradation temperature was noticed in previous sub-chapter. Slight weight loss was also observed for it after 100 °C (**Figure 5B.5**). This is due to moisture absorption by the polar functional groups of carbon dot as a weight loss of about 2% was observed on heating at 105 °C for 3 h without any other change of this nanocomposite. Whereas, in case of nanocomposites with MITH-NH such type of weight loss was not found as the carbon dot as well as Cu_2O nanoparticles were embedded inside the organophilic OMMT layers.

Table 5B.1: Performance of pristine hyperbranched epoxy and its nanocomposites with MITH-NH

Parameter	TAHE20*	MITH-NH1	MITH-NH2	MITH-NH3
Swelling value (%)	24±0.2	22±0.2	22±0.4	21±0.3
Tensile strength (MPa)	40±1.0	53.4±1.4	63.5±1.2	72.5±1.5
Elongation at break (%)	21±1.0	27±0.8	43.5±0.5	54.6±1.4
Toughness (MPa)	540	748	1553	2317
Scratch hardness (kg)	9.0±0.5	>10.0	>10.0	>10.0
Impact resistance (cm)	>100	>100	>100	>100
Bending diameter (mm)	<1	<1	<1	<1
Initial degradation temperature (°C)	267	285	288	296

*As reported in sub-chapter 2A

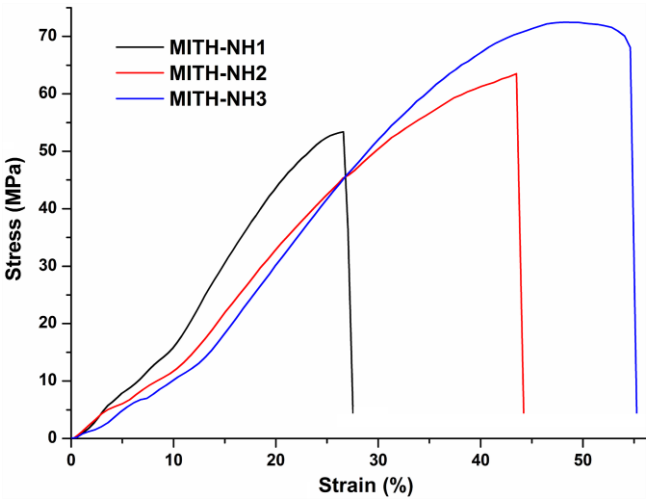

Figure 5B.4: Stress-strain profiles of the nanocomposites

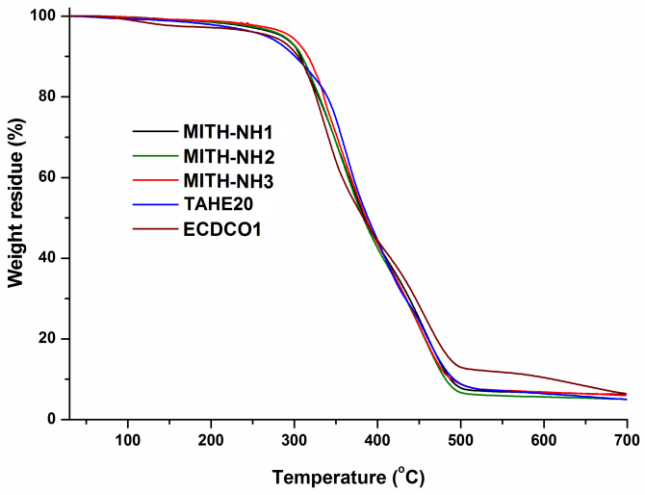

Figure 5B.5: TGA thermograms for pristine hyperbranched epoxy (TAHE20) and its nanocomposites with MITH-NH and carbon dot reduced Cu_2O nanohybrid

5B.3.5. Antimicrobial activity of nanocomposites

Antibacterial test of the nanocomposites was done by well diffusion method. Hyperbranched epoxy/ECDCONC nanocomposites showed significant antimicrobial activity towards different gram positive and gram negative bacteria as shown in **Figure 5B.6 (a-c)**. However, they showed poor antifungal activity against *C. albicans* as shown in **Figure 5B.6d**. Only Cu_2O showed less antimicrobial activity as it is less toxic than Cu or CuO nanoparticles. Again, formation of nanohybrid with carbon dot as well OMMT and fabrication of nanocomposites further reduces toxicity towards fungal strain. Whereas, MITH immobilized nanocomposites exhibited excellent antifungal and antibacterial activity. The bacterial growth curves for MITH-NH1, MITH-NH2, and MITH-NH3 against gram positive and gram negative bacteria are shown in **Figure 5B.7**. From the curves, it is found that the bacterial growths for all the tested bacteria were completely inhibited by the nanocomposites at high dose of MITH-NH. In **Figure 5B.7d**, the increase of *P. aeruginosa* bacterial growth for MITH-NH1 after 10 h is the presence of insufficient amount of biocide, which unable to kill bacterial strain completely. The zones of inhibition against different bacterial strains are shown in **Figure 5B.8**. The antifungal activity of the nanocomposites against *C. albicans* is given in **Figure 5B.9**. From these figures, it is seen that the nanocomposites formed clear inhibition zones against the tested microbes. The diameter of the zone increases with an increase in the amount of MITH-NH in the nanocomposite and MITH-NH3 shows even larger zone of inhibition than the control. The fungal growth curves of the nanocomposites are shown in **Figure 5B.9b**. Where, it is seen that MITH-NH3 completely inhibits the fungal

growth. The strong antimicrobial activity of the nanocomposites is due to the combined effect of inorganic Cu_2O nanoparticles and MITH biocide. In case of Cu_2O, the release of copper ion from the nanocomposites strongly interacts with cell wall of the bacteria. The quantum size of Cu_2O provides large surface area, which makes the interaction strong. The released copper ions of nanocomposites bind with the DNA molecules and lead to disorder structure between the nucleic acids and also disrupts the biochemical process inside the cell of bacteria.[32] In addition to that, carbon dot absorbs visible light as well as near infrared light during the test and emits shorter wavelength of light (300-500 nm), which again excites Cu_2O nanoparticles and forms e^-/h^+ pairs as reported in the previous sub-chapter. These e^-/h^+ pairs react with H_2O and O_2 to produce active oxygen radicals like $^{\cdot}OH$ and $^{\cdot}O_2^-$ which may also participate in killing process of microbes by damaging cell membrane via lipid peroxidation.[43,44] On the other hand, MITH has also been used as a powerful biocide since long period for controlling the growth of microorganisms.[40] However, MITH is highly toxic to environment, mainly marine environment. In this case, immobilization of MITH on the nanoparticles and formation of polymer nanocomposite may reduce its toxicity to the environment. After immobilization into the nanocomposites it is slowly released from the nanoparticles surface (as shown in **Figure 5B.10**) and inhibits the growth of the tested microbes along with the Cu_2O nanoparticles.

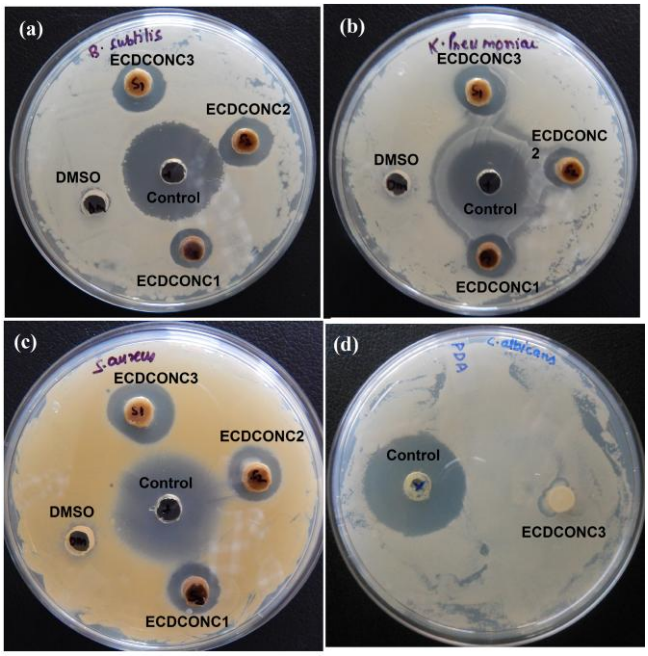

Figure 5B.6: Antimicrobial activity of hyperbranched epoxy nanocomposites with ECDCONC nanohybrid against (a) *Bacillus subtilis*, (b) *Klebsiella pneumonia*, (c) *Staphylococcus aureus* and (d) *Candida albicans*

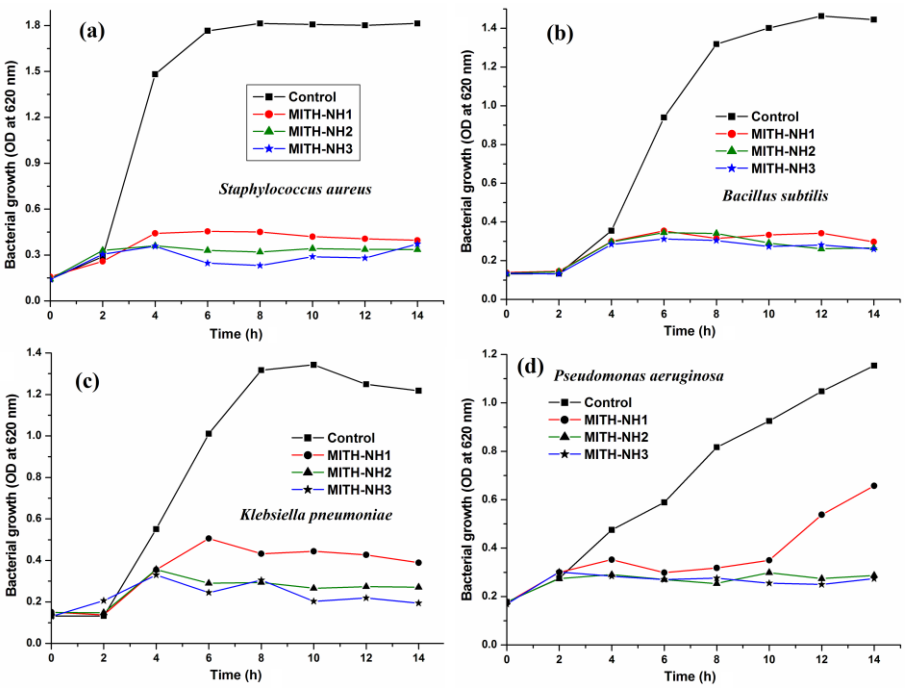

Figure 5B.7: Bacterial growth curves of hyperbranched epoxy nanocomposites with MITH-NH nanohybrid against (a) *Staphylococcus aureus*, (b) *Bacillus subtilis*, (c) *Klebsiella pneumoniae* and (d) *Pseudomonas aeruginosa* bacteria

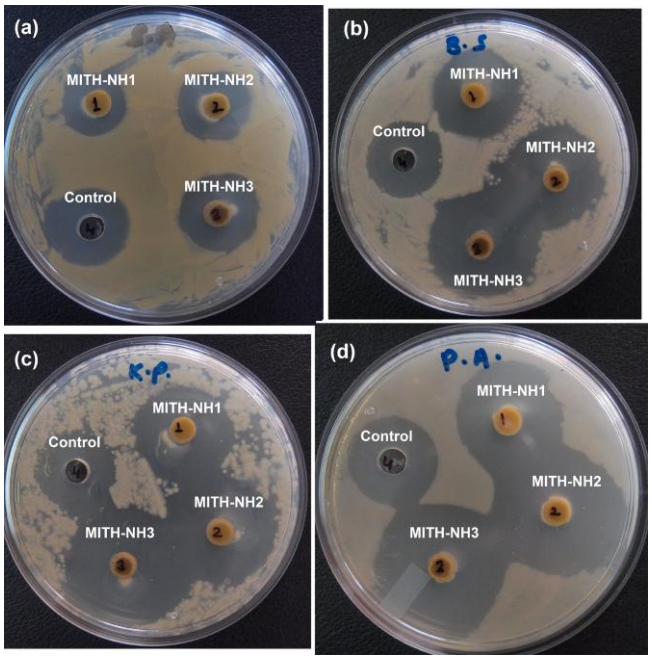

Figure 5B.8: Antibacterial activity of MITH-NH1, MITH-NH2 and MITH-NH3 against (a) *Staphylococcus aureus*, (b) *Bacillus subtilis*, (c) *Klebsiella pneumoniae* and (d) *Pseudomonas aeruginosa* bacteria

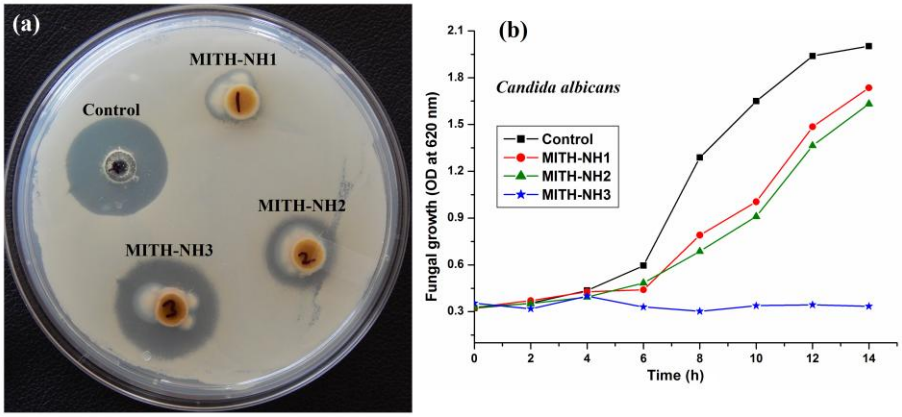

Figure 5B.9: Antifungal activity of MITH-NH1, MITH-NH2 and MITH-NH3 against *Candida albicans*, (a) zone of inhibition and (b) growth curves

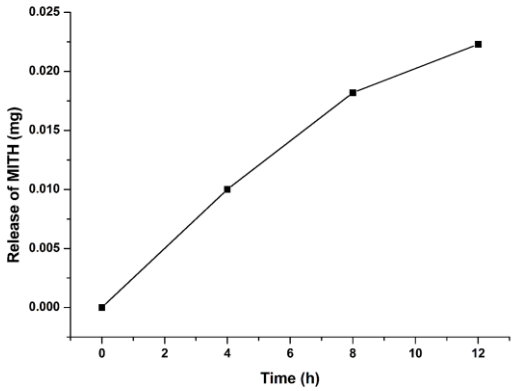

Figure 5B.10: Release profile of MITH biocide for MITH-NH3

5B.3.6. Biofilm formation study

Biofilm formation study was done only for TAHE20 and MITH-NH2 against *C. albicans* fungal strain. The above antimicrobial study of the nanocomposites was done in dispersed state in DMSO. However, the application of the nanocomposites is more important in solid film. So, the biofilm formation study was done on the nanocomposite film surface. From this study, it was found that greater number of fungus adhered on TAHE20 film compared to MITH-NH2 film as shown in **Figure 5B.11**. Thus, it is confirmed that MITH-NH2 inhibited more fungal adherence on the surface of the film as compared to TAHE20, which is due to the presence of MITH as well as Cu_2O nanoparticles on the surface of MITH-NH2 film. The inhibition of biofilm formation by the nanocomposite film is due to the combined effect of

inorganic Cu_2O nanoparticles and MITH biocide. They killed the adhered fungus present on the surface of the film by same mechanism as stated in previous sub-section 5B.3.5.

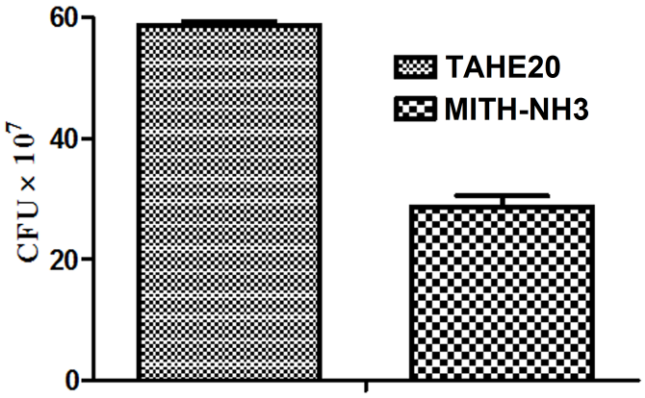

Figure 5B.11: Number of *Candida albicans* adherence on the surface of TAHE20 and MITH-NH2

5B.3.7. Optical properties of nanocomposites

The optical properties like transparency and UV luminescence of the nanocomposites are illustrated in **Figure 5B.12**. From **Figure 5B.12a**, it is seen that the percentage of light transmittance of the pristine thermoset decreased from 90 to 40 at low visible wavelength (500 nm) after formation of MITH-NH3. However, the percent of transmittance is not much effected (changes from 90 to 80) at visible light of long wavelengths (700-800 nm). From the inset picture of **Figure 5B.12a**, it is also found that the transparency and the color of the nanocomposite films (thickness 0.5 mm) also changed with the increase in amount of MITH-NH. The transparency of the pristine film is not much affected after formation of MITH-NH1. However, at high amount of MITH-NH (2 and 3 wt%) the transparency decreases. This is due to the fact that carbon dot as well as Cu_2O nanoparticles can absorb visible light (mainly low wavelength ~500 nm).[8,20,21] The luminescence of the hyperbranched epoxy nanocomposites with 1 wt% carbon dot (ECD1.0, as reported in sub-chapter 4B), 1 wt% carbon dot reduced Cu_2O nanohybrid (ECDCO1.0) and 2 wt% MITH-NH in the visible, short UV (254 nm) and long UV (365 nm) regions are shown in **Figure 5B.12b**. The brown color of the nanocomposites in the visible range was changed into bluish green by illumination with 254 nm UV light and to dark blue at 365 nm UV light. The green and blue color emissions in nanocomposites are due to the corresponding band gaps of quantum size carbon dot as described earlier also. The change of color with the change of wavelength of UV light

is due to the presence of different sizes of carbon dot in the nanocomposites as stated in sub-chapter 4B. The nanoparticles with small and large sizes get excited in the short and long UV region, respectively.

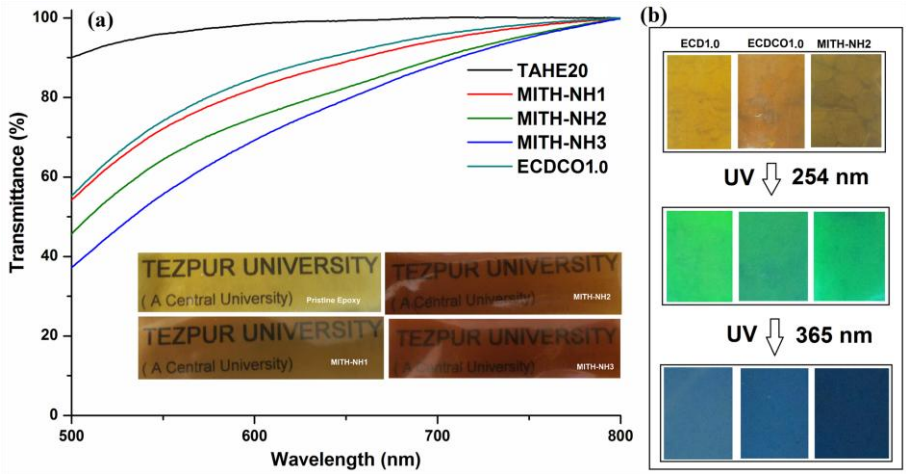

Figure 5B.12: (a) Transparency and (b) optical color emission of the nanocomposites

5B.4. Conclusion

Thus in this sub-chapter, we demonstrated a toughened antimicrobial transparent hyperbranched epoxy nanocomposite with interesting luminescence property. The nanocomposite is formed by incorporation of biocide immobilized OMMT-carbon dot reduced Cu_2O nanohybrid in the epoxy matrix. It is fabricated by a simple protocol at room temperature using the above nanohybrid, obtained by one pot preparative method. The nanocomposite showed excellent antimicrobial activity against both gram positive and gram negative bacteria as well as against a fungus at 3 wt% nanohybrid loading. Immobilization of organic biocide on OMMT-carbon dot reduced Cu_2O nanohybrid resulted advanced antimicrobial material against tested microbes. Thus, this work contributes a light in the field of advanced antimicrobial functional thermosetting material.

References

1. Roy, B., et al. Silver-embedded modified hyperbranched epoxy/clay nanocomposites as antibacterial materials, *Bioresour. Technol.* **127**, 175--180, 2013.
2. Mahapatra, S. S. & Karak, N. Hyperbranched polyamine/Cu nanoparticles for epoxy thermoset, *J. Macromol. Sci., Pure Appl. Chem*. **46**, 296--303, 2009.
3. Karak, N., et al. Catalytically active vegetable-oil-based thermoplastic hyperbranched polyurethane/silver nanocomposites, *Macromol. Mater. Eng*. **294** (2), 159--169, 2009.

4. Shi, H., et al. Synthesis and characterization of novel plasmonic Ag/AgX-CNTs (X = Cl, Br, I) nanocomposite photocatalysts and synergetic degradation of organic pollutant under visible light, *ACS Appl. Mater. Interfaces* **5**, 6959--6967, 2013.
5. Sun, L. et al. Preparation and characterization of polypyrrole/TiO_2 nanocomposites by reverse microemulsion polymerization and its photocatalytic activity for the degradation of methyl orange under natural light, *Polym. Compos*. **34**, 1076--1080, 2013.
6. Kaur, J., et al. Photocatalytic degradation of methyl orange using ZnO nanopowders synthesized via thermal decomposition of oxalate precursor method, *Physica B* **416**, 33--38, 2013.
7. Tu, K., et al. Portable visible-light photocatalysts constructed from Cu_2O nanoparticles and graphene oxide in cellulose matrix, *J. Phys. Chem. C* **118**, 7202--7210, 2014.
8. Li, H., et al. Carbon quantum dots/Cu_2O composites with protruding nanostructures and their highly efficient (near) infrared photocatalytic behavior, *J. Mater. Chem*. **22**, 17470--17475, 2012.
9. Tang, J., et al. Efficient photocatalytic decomposition of organic contaminants over $CaBi_2O_4$ under visible-light irradiation, *Angew. Chem. Int. Ed*. **43**, 4463--4466, 2004.
10. Aragay, G., et al. Nanomaterials for sensing and destroying pesticides, *Chem. Rev*. **112**, 5317--5338, 2012.
11. Kisch, H. Semiconductor photocatalysis mechanistic and synthetic aspects, *Angew. Chem. Int. Ed*. **52**, 812--847, 2013.
12. Kang, Z., et al. Silicon quantum dots: A general photocatalyst for reduction, decomposition, and selective oxidation reactions, *J. Am. Chem. Soc*. **129**, 12090--12091, 2007.
13. Copley, S. D. Evolution of efficient pathways for degradation of anthropogenic chemicals, *Nat. Chem. Biol*. **5**, 559--566, 2009.
14. Prasad, G. K., et al. Photocatalytic degradation of paraoxon-ethyl in aqueous solution using titania nanoparticulate film, *Thin Solid Films* **520**, 5597--5601, 2012.
15. Mattozzi, M. D. L. P., et al. Mineralization of Paraoxon and its use as a sole c and p source by a rationally designed catabolic pathway in *Pseudomonas putida*, *Appl. Environ. Microbiol*. **72**, 6699--6706, 2006.
16. Deo, M., et al. Cu_2O/ZnO hetero-nanobrush: hierarchical assembly, field emission and photocatalytic properties, *J. Mater. Chem*. **22**, 17055--17062, 2012.

17. Abboud, Y., et al. Biosynthesis, characterization and antimicrobial activity of copper oxide nanoparticles (CONPs) produced using brown alga extract (*Bifurcaria bifurcata*), *Appl. Nanosci*. **4**, 571--576, 2014.
18. Yin, M., et al. Copper oxide nanocrystals, *J. Am. Chem. Soc*. **127**, 9506--9511, 2005.
19. Dey, D., et al. Carbon dot reduced palladium nanoparticles as active catalysts for carbon-carbon bond formation, *Dalton Trans*. **42**, 13821--13825, 2013.
20. Li, H., et al. Carbon nanodots: synthesis, properties and applications, *J. Mater. Chem*. **22**, 24230--24253, 2012.
21. Li, H., et al. Water-soluble fluorescent carbon quantum dots and photocatalyst design, *Angew. Chem. Int. Ed*. **49**, 4430--4434, 2010.
22. Kalidindi, S. B., et al. Nanostructured Cu and Cu@Cu_2O core shell catalysts for hydrogen generation from ammonia-borane, *Phys. Chem. Chem. Phys*. **10**, 5870--5874, 2008.
23. He, P., et al. Size-controlled preparation of Cu_2O octahedron nanocrystals and studies on their optical absorption, *J. Colloid Interface Sci*. **284**, 510--515, 2005.
24. Swarnkar, R. K., et al. Effect of aging on copper nanoparticles synthesized by pulsed laser ablation in water: structural and optical characterizations, *Bull. Mater. Sci*. **34**, 1363--1369, 2011.
25. Roy, B., et al. Modified hyperbranched epoxy/clay nanocomposites: A study on thermal, antimicrobial and biodegradation properties, *Int. J. Mater. Res*. **105**, 296--307, 2014.
26. Rai, A., et al. Antibiotic mediated synthesis of gold nanoparticles with potent antimicrobial activity and their application in antimicrobial coatings, *J. Mater. Chem.* **20**, 6789--6798, 2010.
27. Wu, Y., et al. Long-term and controlled release of chlorhexidine-copper (II) from organically modified montmorillonite (OMMT) nanocomposites, *Mater. Sci. Eng. C* **33**, 752--757, 2013.
28. Sharma, V. K., et al. Silver nanoparticles: green synthesis and their antimicrobial activities, *Adv. Colloid Interface Sci*. **145**, 83--96, 2009.
29. Stewart, M., et al. Antifouling activity of synthetic γ-hydroxybutenolides, *Int. Biodeterior. Biodegradation* **88**, 176--184, 2014.
30. Usman, M. S., et al. Synthesis, characterization, and antimicrobial properties of copper nanoparticles, *Int. J. Nanomedicine* **8**, 4467--4479, 2013.
31. Ren, G., et al. Characterisation of copper oxide nanoparticles for antimicrobial applications, *Int. J. Antimicrob. Ag.* **33**, 587--590, 2009.

32. Bagchi, B., et al. In situ synthesis and antibacterial activity of copper nanoparticle loaded natural montmorillonite clay based on contact inhibition and ion release, *Colloids Surf., B* **108**, 358--365, 2013.
33. Tamayo, L. A., Release of silver and copper nanoparticles from polyethylene nanocomposites and their penetration into *Listeria monocytogenes*, *Mater. Sci. Eng. C* **40**, 24--31, 2014.
34. Ren, J., et al. Crystallography facet -dependent antibacterial activity: the case of Cu_2O, *Ind. Eng. Chem. Res*. **50**, 10366--10369, 2011.
35. Lee, Y. J., et al. Morphology-dependent antibacterial activities of Cu_2O, *Mater. Lett.* **65**, 818--820, 2011.
36. Palza, H., et al. Toward tailor-made biocide materials based on poly(propylene)/copper nanoparticles, *Macromol. Rapid Commun*. **31**, 563--567, 2010.
37. Barua, S., et al. Biocompatible high performance hyperbranched epoxy/clay nanocomposite as an implantable material, *Biomed. Mater*. **9**, 025006 (14 p), 2014.
38. Wang, K., et al. Epoxy nanocomposites with highly exfoliated clay: mechanical properties and fracture mechanisms, *Macromolecules* **38**, 788--800, 2005.
39. Park, J. H. & Jana, S. C. Mechanism of exfoliation of nanoclay particles in epoxy-clay nanocomposites, *Macromolecules* **36**, 2758--2768, 2003.
40. LaMarre, T. M., Martin, C. H. and Wilharm, M. T. *Synergistic biocide of 2-(thiocyanomethylthio) benzothiazole with a mixture of 5-chloro-2-methyl-4-isothiazolin-3-one and 2-methyl-4-isothiazolin-3-one*, **US patent 4595691**, 1986.
41. Konwarh, R., et al. Magnetically recyclable, antimicrobial, and catalytically enhanced polymer-assisted "green" nanosystem-immobilized Aspergillus niger amyloglucosidase, *Appl. Microbiol. Biotechnol*. **87**, 1983--1992, 2010.
42. Thakur, S. & Karak, N. Multi-stimuli responsive smart elastomeric hyperbranched polyurethane/reduced graphene oxide nanocomposites, *J. Mater. Chem. A* **2**, 14867--14875, 2014.
43. Bodaghi, H., et al. Evaluation of the photocatalytic antimicrobial effects of a TiO_2 nanocomposite food packaging film by *in vitro* and *in vivo* tests, *LWT-Food Sci. Technol.*, **50**, 702--706, 2013.
44. Lu, Z., et al. Mechanism of antimicrobial activity of CdTe quantum dots, *Langmuir* **24**, 5445--5452, 2008.